Bioorganic & Medicinal Chemistry Letters 26 (2016) 257–261

Contents lists available at ScienceDirect

Bioorganic & Medicinal Chemistry Letters

journal homepage: www.elsevier.com/locate/bmcl

Preclinical characterization of substituted 6,7-dihydro-[1,2,4]triazolo [4,3-*a*]pyrazin-8(5*H*)-one P2X7 receptor antagonists

Michael K. Ameriks *, Hong Ao, Nicholas I. Carruthers, Brian Lord, Suchitra Ravula, Jason C. Rech, Brad M. Savall, Jessica L. Wall, Qi Wang, Anindya Bhattacharya, Michael A. Letavic

Janssen Pharmaceutical Research & Development L.L.C., 3210 Merryfield Row, San Diego, CA 92121, United States

ARTICLE INFO

Article history:
Received 5 November 2015
Revised 12 December 2015
Accepted 15 December 2015
Available online 17 December 2015

Keywords:
P2X7
6,7-Dihydro-[1,2,4]triazolo[4,3-*a*]pyrazin-8(5*H*)-one
Autoradiography
Depression
CNS

ABSTRACT

The synthesis, SAR, and preclinical characterization of a series of substituted 6,7-dihydro[1,2,4]triazolo [4,3]pyrazin-8(5*H*)-one P2X7 receptor antagonists are described. Optimized leads from this series comprise some of the most potent human P2X7R antagonists reported to date (IC_{50}s < 1 nM). They also exhibit sufficient potency and oral bioavailability in rat to enable extensive in vivo profiling. Although many of the disclosed compounds are peripherally restricted, compound **11d** is brain penetrant and upon oral administration demonstrated dose-dependent target engagement in rat hippocampus as determined by ex vivo receptor occupancy with radiotracer **5** (ED_{50} = 0.8 mg/kg).

The P2X7 receptor (P2X7R) is a purinergic ion channel expressed primarily in immune cells. In the periphery, P2X7 receptors are localized on monocytes and macrophages, while in the central nervous system (CNS) P2X7 is found predominantly in glial cells throughout the brain.[1] High concentrations of extracellular ATP are required to activate the P2X7 ion channel and trigger downstream signaling events, most notably secretion of the pro-inflammatory cytokine IL-1 β.[2] Since local ATP levels are frequently elevated in tumor microenvironments and at sites of inflammation or infection, the P2X7 receptor may play a pathophysiological role in amplifying responses to cellular stress.[3] Consequently, P2X7R antagonists have been proposed as potential therapeutics for numerous diseases, ranging from cancer[4] and pain[5] to musculoskeletal,[6] immune,[7] and CNS[8] related disorders.

The human P2X7 receptor was first cloned in 1997,[9] and since then a wide variety of structurally distinct P2X7R antagonists have been reported.[10] At least three compounds have progressed to clinical trials, primarily for the treatment of peripheral inflammatory disorders.[11] However, our longstanding interest in P2X7 relates to the role of IL-1β in the CNS, particularly as a putative contributor to the etiology of mood disorders.[12] In this regard, pyroglutamate **1** appeared especially intriguing because it was reported to be both brain penetrant and moderately potent at the rat P2X7 ion channel (Fig. 1).[13] The latter attribute is notable given the historical challenges in identifying compounds capable of blocking both human and rat P2X7 functional activity.[14] Recently, GlaxoSmithKline also disclosed a series of potent 1,2,4-triazolopiperazine antagonists (hP2X7 IC_{50}s < 10 nM), exemplified by **2**.[15] We have subsequently demonstrated that the introduction of a methyl substituent in the 6-position of this scaffold can dramatically improve potency for rat P2X7 (see compound **3**).[15,16] Related 5,6-bicyclic heterocycles have also appeared in the literature (compounds **4**[17] and **5**[18]), with **5** ([^{3}H] JNJ-54232334) representing a useful radioligand for imaging ex vivo P2X7R binding in mouse and rat brain. Herein, we describe the medicinal chemistry efforts that resulted in the identification of radiotracer **5** and related 6,7-dihydro-[1,2,4]triazolo[4,3-*a*]pyrazin-8(5*H*)-one P2X7 receptor antagonists.

Although the SAR reported for triazole cores **2**–**4** suggested that an exocyclic arylamide moiety was preferred for potency, we anticipated that isosteric *N*-benzyl lactam analogs might also be viable P2X7R antagonists based on analogy to *N*-benzyl amide **1**. To test this hypothesis, 1,2,3-triazolopyridone **8** was prepared in four steps from the known 1,2,3-triazolo[4,5-*c*]pyridine **6** (Scheme 1).[17] The key step in this synthetic route was a chemoselective Ru-catalyzed oxidation of amine **7** to provide the desired lactam **8**.[19] In a similar manner, 1,2,4-triazolopyrazinones **11a** and **11b** were assembled in five steps from previously described triazolopyrazine intermediates **9** and **10**, respectively (Scheme 2).[16] During this sequence, it was necessary to switch from a *tert*-butyl to

* Corresponding author.

http://dx.doi.org/10.1016/j.bmcl.2015.12.052
0960-894X/

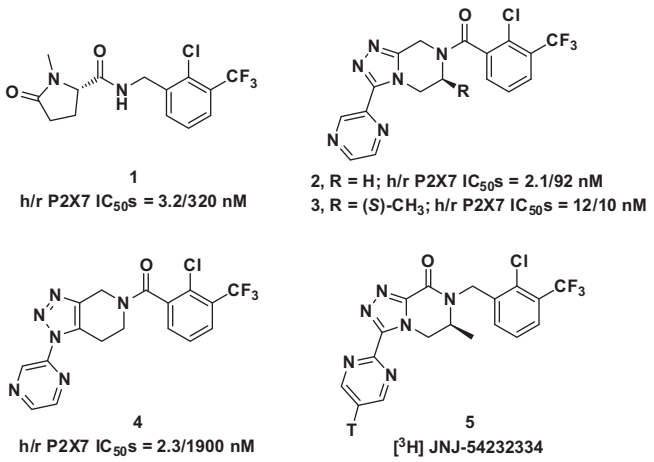

Figure 1. Aryl and *N*-benzyl amide based P2X7 antagonists.

silicon-based carbamate protecting group due to the poor solubility of **9** in the benzylic oxidation step.

Lactams **8**, **11a**, and **11b** were evaluated for their ability to block Bz-ATP induced Ca^{2+} flux in 1321N1 glial cells expressing human or rat P2X7 (Table 1).[20] Although 1,2,3-triazolopyridone **8** is inactive in both cell constructs (IC_{50}s > 10 μM), the analogous 1,2,4-triazole isomer **11a** is a sub-micromolar antagonist of the human P2X7 receptor (IC_{50} = 440 nM). Furthermore, the introduction of a methyl group in the 6-position of this scaffold provided >100-fold improvement in potency for both human and rat P2X7 (compare **11a** and **11b**).[21] Racemate **11b** was separated into individual antipodes **11c** and **11d** using chiral HPLC, and subsequent profiling revealed that only the (−) enantiomer **11d** is a potent P2X7R antagonist. The absolute configuration of **11d** was established by asymmetric synthesis, starting from commercially available (*S*)-1,2-diaminopropane **12** (Scheme 3). It is worth noting that this is the same absolute stereochemistry previously determined for related 6-substituted 1,2,4-triazolopyrazines containing an exocyclic amide (see compound **3**).[16] However, there appear to be important speciation differences in the SAR between the two series: a methyl substituent in the (6*S*)-position dramatically improves potency at the rat P2X7R for both chemotypes, but a similar beneficial effect for the human ortholog is only observed within the lactam series (compare compounds **2** vs **3** and **11a** vs **11d**).[22] As a consequence, even though compound **11d** is only moderately potent against rat P2X7, it is one of the most potent human P2X7 receptor antagonists reported to date.

In order to explore the SAR around the 7-position of **11d**, analogs **11e**–**k** were prepared by alkylating lactam **16** with a variety of substituted benzyl bromides **17** (Scheme 4). Intermediate **16** derived from enantiopure **15**, which in turn was assembled in six steps from commercially available N-Boc-L-alaninol **14** as previously described.[16] Human and rat P2X7 FLIPR data for compounds **11d**–**k** are shown in Table 2. Although the 2,3-dichlorophenyl analog **11e** compares favorably with **11d**, removing substituents from the phenyl ring reduces potency against both human and rat P2X7. However, comparison of **11d** and **11f** with **11g** reveals that monosubstitution in the *meta*-position of the arene is sufficient to achieve single-digit nanomolar potency at the human P2X7 receptor, while additional substitution in the *ortho*-position can provide a synergistic improvement in rat functional activity.

Having established that the (2-chloro-3-trifluoromethyl)benzyl group is a preferred lactam substituent, we held this moiety fixed and optimized the 3-position of the triazole. To this end, compounds **11l**–**t** were prepared by initial activation of amide **13** as an imidate or thioamide, followed by condensation with a variety of aryl and heteroaryl hydrazides (Scheme 3). Due to the highly lipophilic nature of the *N*-benzyl group in the 7-position, the majority of the hydrazide inputs were selected to minimize Log*P*. Gratifyingly, both five- and six-membered heteroaromatic substituents are well tolerated by the human P2X7 receptor (IC_{50}s < 10 nM), but these compounds are also generally 100-fold less potent against rat P2X7 (Table 3). Similar to the SAR trends observed during the optimization of the 7-position, small structural changes in the 3-position dramatically affect rat P2X7 functional activity (compare **11o** with **11p**, **11q** with **11r**, and **11s** with **11t**). However, despite the consistent disparity in potency between human and rat orthologs, four compounds (**11d**, **11m**, **11q**, and **11s**) displayed sufficient P2X7 antagonism in the rat FLIPR assay (IC_{50} < 100 nM) to warrant further evaluation.

All four lead compounds were predicted to be promising CNS candidates based on their high MPO (multiparameter optimization) scores (Table 4). This algorithm utilizes six calculated physicochemical properties (*c*Log*P*, *c*Log*D*, MW, TPSA, HBD, and pK_a) to rate compounds on a scale of zero to six.[23] In general, experimental ADME data support these favorable in silico evaluations, as all four leads exhibit minimal turnover in human and rat liver microsomes, along with low plasma protein binding and encouraging aqueous solubility across a physiologically relevant pH range. However, in the Caco-2 cell permeability assay, only pyrazine **11d** shows comparable rates of transport in both directions (B–A/A–B = 1.1), whereas the remaining three compounds are actively effluxed (B–A/A–B > 10).

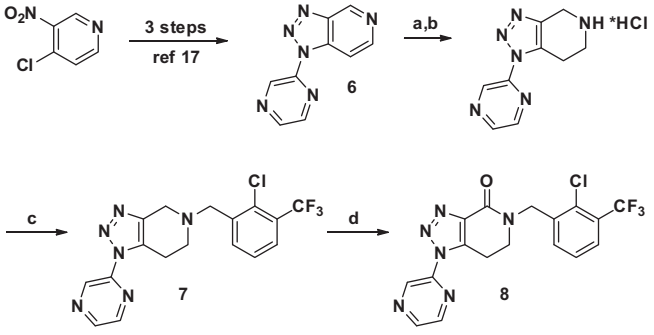

Scheme 1. Synthesis of compound **8**. Reagents and conditions: (a) HCO_2H, Et_3N, 160 °C (36%); (b) 6 N HCl, rt (94%); (c) 2-chloro-3-(trifluoromethyl)benzyl bromide, Et_3N, DMF, rt (82%); (d) cat RuO_2, $NaIO_4$, MeCN/$CHCl_3$/H_2O, rt (43%).

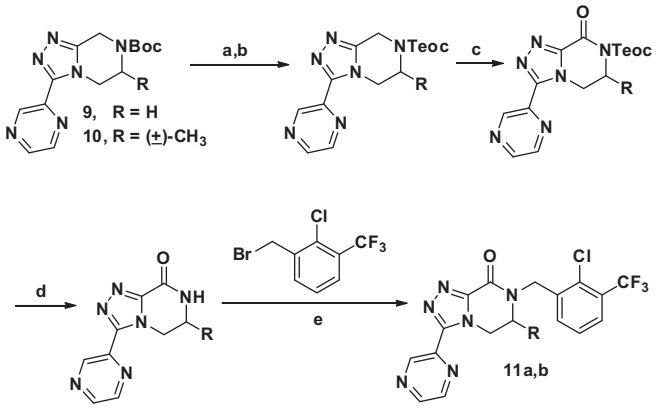

Scheme 2. Synthesis of compounds **11a** and **11b**. Reagents and conditions: (a) 1.25 M HCl/EtOH, DCM, rt (61%); (b) TeocSuc, *i*Pr_2NEt, DMF, rt (57–89%); (c) cat RuO_2, $NaIO_4$, MeCN/$CHCl_3$/H_2O, rt (29–44%); (d) TFA, DCM, rt (71–95%); (e) Cs_2CO_3, DMF, rt (63–79%).

Table 1
In vitro potency of lactams **8**, **11a–d**

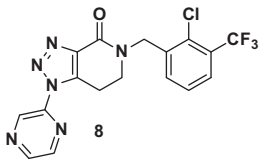

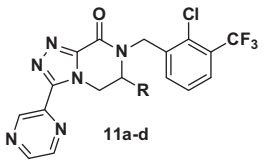

Compound	R	hP2X7 IC_{50}[a] (nM)	rP2X7 IC_{50}[a] (nM)
8	H	>10,000 (n = 1)	>10,000 (n = 1)
11a	H	440 (n = 1)	8670 (n = 1)
11b	(±) CH_3	3.4 ± 0.1	36 ± 16
11c	(+) CH_3	4710 ± 3930	>10,000
11d	(−) CH_3	0.7 ± 0.3	79 ± 39

[a] IC_{50}s determined using a FLIPR Ca^{2+} flux assay. Values represent the mean of at least three experiments run in triplicate, unless otherwise noted. h denotes human, and r is rat.

The Caco-2 assay is generally used as an in vitro screen to predict intestinal absorption, but in the case of compounds **11d**, **11m**, **11q**, and **11s**, rat PK experiments revealed a much stronger association between Caco-2 efflux ratios and brain penetration (Table 5). Whereas all four leads reach micromolar plasma levels following a single 10 mg/kg oral dose, only **11d** partitions effectively into the brain ([brain]/[plasma] = 0.7). The degree of brain penetration also correlates well with receptor occupancy in the hippocampus, which was assessed by ex vivo autoradiography using the competitive P2X7 receptor antagonist [^{3}H] A-804598.[24] In particular, **11d** achieves significant central target engagement, whereas **11q** and **11s** are both peripherally restricted and show little to no receptor occupancy in the brain. However, all of the compounds depicted in Table 5 are orally bioavailable in rat (%F > 80) and possess suitable PK profiles to support further in vivo evaluation. Given their structural similarity and differing tissue distribution in rat, **11d** and **11s** could potentially serve as complementary tool compounds for selectively probing the central and systemic effects of P2X7 antagonism in various preclinical disease models.

To guide further development of **11d** for CNS indications, in vitro and ex vivo P2X7R occupancy dose–responses were obtained in rat brain hippocampal tissue sections. In these studies, pyrazinone **5** was used in place of [^{3}H] A-804598 as the radiotracer due to its reduced non-specific binding in rat brain tissue.[18] Compound **5** is a tritiated derivative of pyrimidine **11m**, which was selected for radiolabeling based on improved physicochemical properties (i.e., free fraction and aqueous solubility) and rat potency compared to **11d**. In rat hippocampal tissue sections, **11d** completely displaced **5** with an IC_{50} = 28 ± 12 nm (Fig. 2).

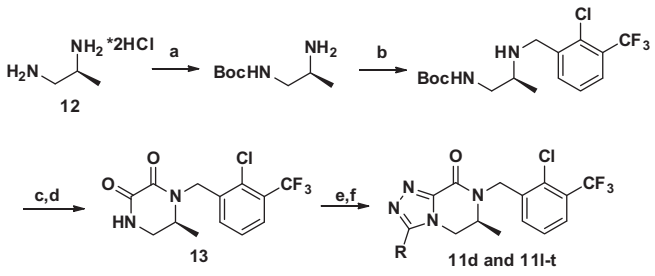

Scheme 3. Synthesis of compounds **11d** and **11l–t**. Reagents and conditions: (a) Boc_2O, NaOH, H_2O/MeOH, 0 °C→rt (42%); (b) 2-chloro-3-trifluoromethylbenzaldehyde, $Na(OAc)_3BH$, DCE, rt (85%); (c) methyl chlorooxoacetate, Et_3N, CH_2Cl_2, 0 °C→rt (97%); (d) 4 N HCl/dioxane, rt, then Et_3N, CH_2Cl_2, rt (100%); (e) $Et_3O^+BF_4^-$, DCM, rt, or Lawesson's reagent, THF, 55 °C (67–99%); (f) $RCONHNH_2$, 1-butanol, 130 °C (27–90%).

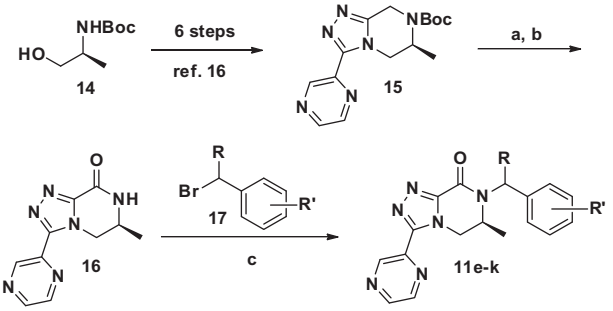

Scheme 4. Synthesis of compounds **11e–k**. Reagents and conditions: (a) cat RuO_2, $NaIO_4$, $MeCN/CHCl_3/H_2O$, rt (48%); (b) TFA, DCM, rt (64%); (c) Cs_2CO_3, DMF, rt (26–76%).

Table 2
In vitro potency of compounds **11d–k**

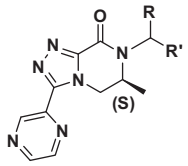

Compound	R	R'	hP2X7 IC_{50}[a] (nM)	rP2X7 IC_{50}[a] (nM)
11d	H	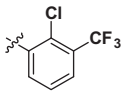	0.7 ± 0.3	79 ± 39
11e	H	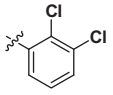	1.0 ± 0.1	103 ± 11
11f	H	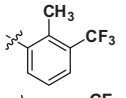	3.4 ± 1.5	506 ± 209
11g	H	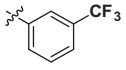	3.6 ± 1.4	4140 ± 990
11h	H		216 ± 28	>10,000
11i	H		72 ± 21	2384 ± 879
11j	H		6960 ± 2300	>10,000
11k	(±) CH_3	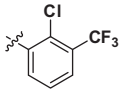	65 ± 20	2690 ± 317

[a] IC_{50}s determined using a FLIPR Ca^{2+} flux assay. Values represent the mean of at least three experiments run in triplicate, unless otherwise noted. h denotes human, and r is rat.

Similarly, following oral administration, **11d** exhibited dose-dependent ex vivo P2X7 receptor occupancy in rat brain, reaching full occupancy at 10 mg/kg (Fig. 3). The calculated ED_{50} (0.8 mg/kg) corresponds to plasma and brain EC_{50}s of 62 ng/mL and 66 ng/mL, respectively. However, accounting for rat brain and plasma protein binding (95.4%/90.4%), the unbound brain-to-plasma partition ratio ($K_{p\ u,u}$) at this dose is 0.51, which suggests that brain uptake of **11d** may be limited by efflux mechanisms.

Table 3
In vitro potency of compounds **11d** and **11l–t**

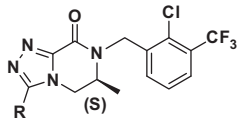

Compound	R	hP2X7 IC_{50}[a] (nM)	rP2X7 IC_{50}[a] (nM)
11d		0.7 ± 0.3	79 ± 39
11l		3.8 ± 1.5	>10,000
11m		0.5 ± 0.06	32 ± 7
11n		0.5 ± 0.08	350 ± 34
11o	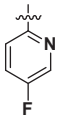	0.7 ± 0.2	380 ± 220
11p	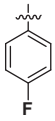	0.2 ± 0.02	3610 ± 2280
11q		1.9 ± 1.2	88 ± 74
11r		4.3 ± 1.7	6670 ± 2110
11s		0.6 ± 0.4	7.1 ± 3.6
11t	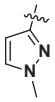	4.2 ± 1.5	960 ± 720

[a] IC_{50}s determined using a FLIPR Ca^{2+} flux assay. Values represent the mean of at least three experiments run in triplicate, unless otherwise noted. h denotes human, r is rat, and m is mouse.

Table 4
In vitro ADME/DMPK data for lead compounds

Compound	CNS MPO	HLM/RLM stability[a]	%PPB[b] (h/r)	Solubility[c] (pH 2/pH 7)	Caco-2[d] (A–B/B–A)
11d	5.6	0.4/0.4	87/90	89/56	47/50
11m	5.6	<0.3/<0.2	79/83	176/201	4.4/64
11q	5.5	0.3/0.3	78/83	>400/375	6.2/73
11s	5.5	<0.3/0.2	92/90	41/95	5.4/65

[a] Stability in human and rat liver microsomes at 1 μM. Data reported as extraction ratios.
[b] Plasma protein binding for human/rat reported as % bound at 1 μM.
[c] Aqueous equilibrium solubility at pH 2 and pH 7 in μM.
[d] Data shown are P_{app} A–B/B–A($\times 10^{-6}$) cm/s.

In addition to being a very potent human P2X7R antagonist, **11d** appears extremely selective. The compound lacks affinity for the hERG channel (IC_{50} > 10 μM, dofetilide binding assay), does not exhibit any cross-reactivity in a Eurofins Cerep panel of ion-channels and GPCRs (0/50 > 50% inhibition at 1 μM), and demonstrates minimal potential for drug–drug interactions (2C19 IC_{50} = 7.2 μM, all other CYPs > 10 μM). However, despite this promising preclinical profile, further development of **11d** was ultimately suspended in favor of antagonists from related series due to their superior potency in the rat ex vivo P2X7R occupancy assay.

In summary, we have described the synthesis, SAR, and preclinical characterization of a series of 6,7-dihydro[1,2,4]triazolo[4,3]pyrazin-8(5*H*)-one P2X7 receptor antagonists. The introduction of a methyl group in the 6-position dramatically improved potency in both human and rat FLIPR Ca^{2+} flux assays. Many of the disclosed

Table 5
In vivo profile of lead compounds

Compound	Rat PK parameters[a]				Rat BBB[b]	
	V_{ss} (L/kg)	Cl (mL/min/kg)	$T_{1/2}$ (h)	%F	B/P @ T_{max}[c]	P2X7 R.O. @ T_{max}[d]
11d	1.5	19	1.0	125	672/945	78
11m	3.3	11	4.8	80	116/2788	41
11q	5.0	21	2.8	82	43/1064	0
11s	4.2	13	3.9	81	41/1311	3

[a] Compounds dosed as solutions in 20% HP-β-CD at 1 mg/kg (iv) and 5 mg/kg (po).
[b] Compounds dosed at 10 mpk, po in Sprague Dawley rats (n = 2 or 3).
[c] Brain (B) and plasma (P) concentrations listed in ng/mL.
[d] P2X7 receptor occupancy in rat hippocampus as measured by ex vivo autoradiography using [^{3}H] A-804598 as the radiotracer.[24]

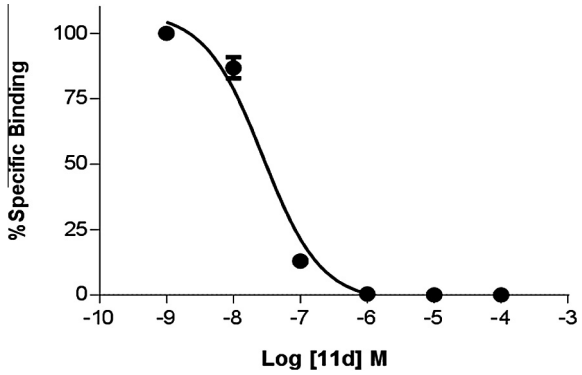

Figure 2. Competition of [^{3}H] **5** binding by **11d** in membranes from rat hippocampus. Data are expressed as mean ± SD from n = 3 replicates per data point.

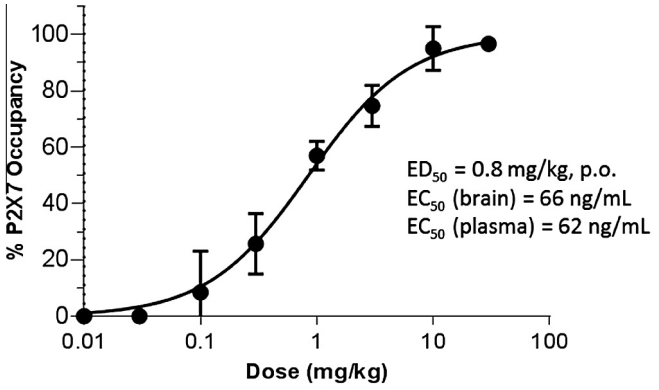

Figure 3. Ex vivo P2X7 receptor occupancy with compound **11d** in rat brain: dose dependency following po administration (n = 3 per dose ± SEM). P2X7 occupancy was measured 30 min after drug administration using compound **5** as the radiotracer.

compounds have outstanding physicochemical properties, which helped guide the identification of **5** as a novel radioligand for imaging ex vivo P2X7R binding in rat brain. Optimized leads from this series are orally bioavailable in rat and possess sufficient PK profiles to enable further in vivo profiling. In particular, **11d** is a potent, selective, and brain-penetrant P2X7R antagonist that exhibits dose-dependent target engagement in rat hippocampus following oral administration.

References and notes

1. (a) Burnstock, G.; Knight, G. E. *Int. Rev. Cytol.* **2004**, *240*, 31; (b) Sperlagh, B.; Vizi, E. S.; Wirkner, K.; Illes, P. *Prog. Neurobiol.* **2006**, *78*, 327.
2. (a) Solle, M.; Labasi, J.; Perregaux, D. G.; Stam, E.; Petrushova, N.; Koller, B. H.; Griffiths, R. J.; Gabel, C. A. *J. Biol. Chem.* **2001**, *276*, 125; (b) Munoz-Planillo, R.; Kuffa, P.; Martinez-Colon, G.; Smith, B. L.; Rajendiran, T. M.; Nunez, G. *Immunity* **2013**, *38*, 1142.
3. (a) Bartlett, R.; Stokes, L.; Sluyter, R. *Pharmacol. Rev.* **2014**, *66*, 638; (b) Ferrari, D.; Pizzirani, C.; Adinolfi, E.; Lemoli, R. M.; Curti, A.; Idzko, M.; Panther, E.; DiVirgilio, F. *J. Immunol.* **2006**, *176*, 3877.
4. Roger, S.; Jelassi, B.; Couillin, I.; Pelegrin, P.; Besson, P.; Jiang, L.-H. *Biochim. Biophys. Acta* **2015**, *1848*, 2584.
5. Bele, T.; Fabbretti, E. *Curr. Med. Chem.* **2015**, *22*, 845.
6. Jorgensen, N. R.; Syberg, S.; Ellegaard, M. *Curr. Med. Chem.* **2015**, *22*, 902.
7. (a) Di Virgilio, F. *Curr. Med. Chem.* **2015**, *22*, 866; (b) Mehta, N.; kaur, M.; Singh, M.; Chand, S.; Vyas, B.; Silakari, P.; Singh Bahia, M.; Silakari, O. *Bioorg. Med. Chem.* **2014**, *22*, 54.
8. (a) Burnstock, G. *Curr. Med. Chem.* **2015**, *22*, 819; (b) Chrovian, C.; Rech, J. C.; Bhattacharya, A.; Letavic, M. A. *Prog. Med. Chem.* **2014**, *53*, 65.
9. Rassendren, F.; Buell, G. N.; Virginio, C.; Collo, G.; North, R. A.; Surprenant, A. *J. Biol. Chem.* **1997**, *272*, 5482.
10. (a) Baudelet, D.; Lipka, E.; Millet, R.; Ghinet, A. *Curr. Med. Chem.* **2015**, *22*, 713; (b) Guile, S. D.; Alcaraz, L.; Birkinshaw, T. N.; Bowers, K. C.; Ebden, M. R.; Furber, M.; Stocks, M. J. *J. Med. Chem.* **2009**, *52*, 3123.
11. (a) Ali, Z.; Laurijssens, B.; Ostenfeld, T.; McHugh, S.; Stylianou, A.; Scott-Stevens, P.; Hosking, L.; Dewit, O.; Richardson, J. C.; Chen, C. *Br. J. Clin. Pharmacol.* **2012**, *75*, 197; (b) Stock, T. C.; Bloom, B. J.; Wei, N.; Ishaq, S.; Park, W.; Wang, X.; Gupta, P.; Mebus, C. A. *J. Rhematol.* **2012**, *39*, 720; (c) Eser, A.; Colombel, J. F.; Rutgeerts, P.; Vermeire, S.; Vogelsang, H.; Braddock, M.; Persson, T.; Reinisch, W. *Inflamm. Bowel Dis.* **2015**, *21*, 2247; (d) Keystone, E. C.; Wang, M. M.; Layton, M.; Hollis, S.; McInnes, I. B. *Ann. Rheum. Dis.* **2012**, *71*, 1630.
12. (a) Sperlagh, B.; Illes, P. *Trends Pharmacol. Sci.* **2014**, *35*, 537; (b) Koo, J. W.; Duman, R. S. *Proc. Natl. Acad. Sci. U.S.A.* **2008**, *105*, 751.
13. Abdi, M. H.; Beswick, P. J.; Billinton, A.; Chambers, L. J.; Charlton, A.; Collins, S. D.; Collis, K. L.; Dean, D. K.; Fonfria, E.; Gleave, R. J.; Lejeune, C. L.; Livermore, D. G.; Medhurst, S. J.; Michel, A. D.; Moses, A. P.; Page, L.; Patel, S.; Roman, S. A.; Senger, S.; Slingsby, B.; Steadman, J. G. A.; Stevens, A. J.; Walter, D. S. *Bioorg. Med. Chem. Lett.* **2010**, *20*, 5080.
14. (a) Caseley, E. A.; Muench, S. P.; Baldwin, S. A.; Simmons, K.; Fishwick, C. W.; Jiang, L.-H. *Bioorg. Med. Chem. Lett.* **2015**, *25*, 3164; (b) Michel, A. D.; Clay, W. C.; Ng, S. W.; Roman, S.; Thompson, K.; Condreay, J. P.; Hall, M.; Holbrook, J.; Livermore, D.; Senger, S. *Br. J. Pharmacol.* **2008**, *155*, 738.
15. Dean, D. K.; Munoz-Muriedas, J.; Sime, M.; Steadman, J. G. A.; Thewlis, R. E. A.; Trani, G.; Walter, D. S. PCT Int. Appl. WO2010125102 A1 20101104, 2010.
16. Rudolph, D. A.; Alcazar, J.; Ameriks, M. K. *Bioorg. Med. Chem. Lett.* **2015**, *25*, 3157.
17. Savall, B. M.; Wu, D.; De Angelis, M.; Carruthers, N. I.; Ao, H.; Wang, Q.; Lord, B.; Bhattacharya, A.; Letavic, M. A. *ACS Med. Chem. Lett.* **2015**, *6*, 671.
18. Lord, B.; Ameriks, M. K.; Wang, Q.; Fourgeaud, L.; Vliegen, M.; Verluyten, W.; Haspeslagh, P.; Carruthers, N. I.; Lovenberg, T. W.; Bonaventure, P.; Letavic, M. A.; Bhattacharya, A. *Eur. J. Pharmacol.* **2015**, *765*, 551.
19. Weber, A. E.; Ashton, W. T. PCT Int. Appl. WO2006023750 A2 20060302, 2006.
20. All of the compounds were tested at 10 μM in a human peripheral blood monocyte (HPBMC) assay prior to determining IC_{50}s in FLIPR. The protocols for the HPBMC and FLIPR assays are described in the following references: (a) Letavic, M. A.; Lord, B.; Bischoff, F.; Hawryluk, N. A.; Pieters, S.; Rech, J. C.; Sales, Z.; Velter, A. I.; Ao, H.; Bonaventure, P.; Contreras, V.; Jiang, X.; Morton, K. L.; Scott, B.; Wang, Q.; Wickenden, A. D. *ACS Med. Chem. Lett.* **2013**, *31*, 105; (b) Bhattacharya, A.; Wang, Q.; Ao, H.; Shoblock, J. R.; Lord, B.; Aluisio, L.; Fraser, I.; Nepomuceno, D.; Neff, R. A.; Welty, N.; Lovenberg, T. W.; Bonaventure, P.; Wickenden, A. D.; Letavic, M. A. *Br. J. Pharmacol.* **2013**, *170*, 624.
21. For reviews on dramatic effects of methyl substituents in drug discovery, see (a) Schonherr, H.; Cernak, T. *Angew. Chem., Int. Ed.* **2013**, *52*, 12256; (b) Leung, C. S.; Leung, S. S. F.; Tirado-Rives, J.; Jorgensen, W. L. *J. Med. Chem.* **2012**, *55*, 4489.
22. A complete analysis describing the conformational effects of chiral substituents on potency at human and rat P2X7 for compounds related to **3**–**5** will be published separately.
23. Wager, T. T.; Hou, X.; Verhoest, P. R.; Villalobos, A. *ACS Chem. Neurosci.* **2010**, *1*, 435.
24. (a) Able, S. L.; Fish, R. L.; Bye, H.; Booth, L.; Logan, Y. R.; Nathaniel, C.; Hayter, P.; Katugampola, S. D. *Br. J. Pharmacol.* **2011**, *162*, 405; (b) Donnelly-Roberts, D. L.; Namovic, M. T.; Surber, B.; Vaidyanathan, S. X.; Perez-Medrano, A.; Wang, Y.; Carroll, W. A.; Jarvis, M. F. *Neuropharmacology* **2009**, *56*, 223.